EXPERIMENTAL DETERMINATION OF STRESSES IN A SHIP'S BOTTOM STRUCTURE

James Conrad Card

EXPERIMENTAL DETERMINATION OF STRESSES IN A SHIP'S BOTTOM STRUCTURE

by

JAMES CONRAD CARD

S.B., U.S. Coast Guard Academy

(1964)

SUBMITTED IN PARTIAL FULFILLMENT

OF THE REQUIREMENTS FOR THE

DEGREES OF MASTER OF SCIENCE

IN NAVAL ARCHITECTURE AND MARINE ENGINEERING

AND MECHANICAL ENGINEERING

at the

MASSACHUSETTS INSTITUTE OF

TECHNOLOGY

May, 1970

EXPERIMENTAL DETERMINATION OF STRESSES IN A SHIP'S BOTTOM STRUCTURE

by

James Conrad Card

Submitted to the Department of Naval Architecture and Marine Engineering and to the Department of Mechanical Engineering on 21 May 1970 in partial fulfillment of the requirements for the degrees of Master of Science in Naval Architecture and Marine Engineering and of Master of Science in Mechanical Engineering.

Abstract

An attempt is made to verify second order orthotropic plate theory using a Plexiglas model loaded laterally and in the plane of the plate. The design and construction of the model, loading system, support system and instrumentation are discussed in detail.

The experiments did not verify second order orthotropic plate theory. The main reason was the inability of the boundary condition members to apply the designed boundary conditions to the plate. Further attempts to verify the theory are possible with the same apparatus if boundary modifications are made.

Thesis Supervisor: Alaa E. Mansour

Title: Assistant Professor of Naval Architecture

ACKNOWLEDGEMENTS

I would like to express my sincere appreciation to Professor A. Mansour for his advice, guidance and criticism throughout the work on this thesis. His office was always open for discussion and he gave me the encouragement I needed to complete the work.

I would also like to thank Dr. Murray and Bob Walters for their advice on strain gages and associated circuitry.

My wife and children deserve a special thanks for giving me the family support of love and understanding which I needed to complete this thesis.

TABLE OF CONTENTS

NOMENCLATURE

x	ordinate in logitudinal direction
y	ordinate in transverse direction
a,b	plate length and breadth, respectively
h	plate thickness
w	vertical deflection
D_x, D_y	flexural rigidity of the orthotropic plate in the x or y directions, respectively
H	effective torsional rigidity of the orthotropic plate
ν_x, ν_y	Poisson's ratio of the orthotropic plate in the x or y directions, respectively
E	modulus of elasticity
M_x, M_y	bending moments in the orthotropic plate acting around a line perpendicular to the x or y axis, respectively, per unit width
M_{x_o}, M_{y_o}	bending moments in the orthotropic plate assuming that $\nu_x = \nu_y = 0$.
q	uniform lateral load
N_x	uniform inplane load
$\rho = \frac{a}{b}\sqrt[4]{\frac{D_y}{D_x}}$	virtual aspect ratio of the orthotropic plate
$\eta = \frac{H}{D_x D_y}$	torsion coefficient of the orthotropic plate
$\alpha = \frac{w}{(\frac{qb^4}{D_y})}$	non-dimensional deflection
$\beta = \frac{M_{x_o}}{qb^2\sqrt{\frac{D_x}{D_y}}}$	non-dimensional moment around a line perpendicular to the x-axis, assuming $\nu_y = 0$.

$\gamma = \frac{M_{y_o}}{qb^2}$	non-dimensional moment around a line perpendicular to the y-axis, assuming $\nu_x = 0$.
$N^* = \frac{\pi^2 \sqrt{D_x D_y}}{b^2}$	parameter used in computation of the inplane load in orthotropic plate
$\beta' = \frac{M_x}{qb^2 \sqrt{\frac{D_x}{D_y}}}$	non-dimensional moment around a line perpendicular to the x-axis
$\gamma' = \frac{M_y}{qb^2}$	non-dimensional moment around a line perpendicular to the y-axis
r_a, r_b	bending lever arms in the x- and y-directions, respectively

INTRODUCTION

A ship's structure can be thought of as the material which provides strength and stiffness to withstand the loads the ship may be expected to experience. The structure can be divided into two groups, the hull girder and the transverse bulkheads. The primary loading of the hull girder comes from bending of the ship as a beam. In addition to the longitudinal loading from bending, the bottom portion of the hull girder is loaded normally due to the hydrostatic pressure of the water.

Design of ship's structures, including the bottom structure, in the past has been based primarily on experience with previous designs and "safe rule of thumb" engineering. However, recently more rigorous engineering approaches have been possible with the aid of the computer, and it appears that more engineering and less art will be applied in ship structure design.

In the design of bottom structures, as in all other structures, the primary objectives are to provide adequate strength and stiffness while limiting the cost of material and fabrication. Optimization of the structure leads to real savings, since structure redundancy may be considered exchanged pound for pound with cargo, and based on a 25 year life expectancy any savings in weight would be economically attractive.

The use of more sound engineering principles in designing the bottom structure is not an easy problem, because the

structure is fairly complex consisting of outer and inner bottom plating, transverse frames (floors) and a stiff longitudinal member at the center (keel) with or without additional longitudinals. (See Figure 1) Attempts to use a more analytical approach began with Schnadel in 1928 when he applied the orthotropic plate theory developed by Huber to a ship's structure.[1] An orthotropic plate is a homogeneous plate whose elastic properties are different in two mutually orthogonal directions in the plane of the plate. Schnadel derived a differential equation for an idealized ship structure subjected to a uniform bending load with the longitudinals and keel being equally stiff.

Schade from 1938-1941[1,2,3,4] extended orthotropic plate theory to include the case of a plate panel with a centerline stiffener and with boundary conditions that exist in the ship. His paper in 1941[4] gives a simple and practical design method for plating subjected to a uniform bending load. The method is general, in that it is applicable to four types of plates ranging from cross stiffened plating to plating with no stiffeners, and four sets of boundary conditions ranging from all edges simply supported to all edges clamped. The design information is presented in the form of curves.

Schade's curves have been used considerably in the design of cross stiffened plating, however the loading on a ship's bottom structure is not only that of uniform bending, but also the inplane load due to the bending of the ship as a beam. This longitudinal stress was superimposed on the uniform

bending stress to arrive at the total stress in the bottom structure. This approach is known as the linear or first order theory and is currently considered acceptable.

First order theory doesn't take into account the deflection of the plate caused by inplane loads. Linearized theory or second order theory takes this deflection into account and in essence couples the effect of longitudinal bending stresses (primary stresses) and uniform bending stresses (secondary stresses). In 1966 Mansour[5] solved the same type of orthogonal plating problem as did Schade, however he used the more accurate second order theory. The aim of Mansour's work was to "get design curves representing deflections and stresses for a wide range of parameters that specify the elastic characteristics of the plate and its loading condition. The final goal was a rational basis for designing ship bottom plating." The results are presented in the form of curves useful to the designer.

Any theoretical solution needs to be checked to some extent experimentally before it can be used with confidence in design. The aim of this thesis is to check Mansour's theoretical work with a meaningful experiment. To complete the background for the experimental work a brief summary of the linearized solution of orthotropic plates as given by Mansour is presented.

The basic differential equation describing the deflection surface of an orthotropic plate under combined action of lateral and inplane loads within the scope of the linearized

analysis

$$D_x \frac{\partial^4 w}{\partial x^4} + 2H \frac{\partial^4 w}{\partial x^2 \partial y^2} + D_y \frac{\partial^4 w}{\partial y^4} = q \pm N_x \frac{\partial^2 w}{\partial x^2}$$

The solution was carried out for four sets of boundary conditions:

Case I: All edges simply supported.

Case II: The two edges loaded with inplane loads simply supported the other two edges fixed.

Case III: The two edges loaded with inplane loads fixed, the other two simply supported.

Case IV: All edges fixed.

The deflection and moments in the plate field are functions of the following variables:

$$w = f(x,y,a,b,D_x,D_y,H,q,N_x)$$

$$M_x = f(x,y,a,b,D_x,D_y,H,q,N_x,\nu_y)$$

$$M_y = f(x,y,a,b,D_x,D_y,H,q,N_x,\nu_x)$$

By considering a fixed location in the plate field, w can be reduced to a function of 7 variables and M_x and M_y as functions of 8 variables. Equations of moments at any point in the plate are:

$$M_x = -D_x\left(\frac{\partial^2 w}{\partial x^2} + \nu_y \frac{\partial^2 w}{\partial y^2}\right)$$

$$M_y = -D_y\left(\frac{\partial^2 w}{\partial y^2} + \nu_x \frac{\partial^2 w}{\partial x^2}\right)$$

In order to reduce the variables to present the results effectively three steps were taken:

(1) Solutions in the curves are given for M_x and M_y with ν_y and $\nu_x = 0$.

$$M_{x_o} = -D_x \frac{\partial^2 w}{\partial x^2} \qquad M_{y_o} = -D_y \frac{\partial^2 w}{\partial y^2}$$

(2) The dimensional variables are grouped non-dimensionally so w, M_{x_o} and M_{y_o} can be represented as functions of three non-dimensional parameters only.

$$\frac{w}{\left(\frac{qb^4}{D_y}\right)} = \alpha\left(\rho, \eta, \frac{N_x}{N^*}\right)$$

$$\frac{M_{x_o}}{qb^2 \frac{D_x}{D_y}} = \beta\left(\rho, \eta, \frac{N_x}{N^*}\right)$$

$$\frac{M_{y_o}}{qb^2} = \gamma\left(\rho, \eta, \frac{N_x}{N^*}\right)$$

where

$$\rho = \frac{a}{b} \sqrt[4]{\frac{D_x}{D_y}}$$

$$\eta = \frac{H}{D_x D_y}$$

$$N^* = \frac{\pi^2 D_x D_y}{b^2}$$

(3) A relation between ρ, η and $\frac{N_x}{N^*}$ is found in the critical load and hence the three non-dimensional

parameters are reduced to two.

The equations are then solved for each of the first three boundary conditions and loadings. α, β and γ are found in each case as functions of ρ, η and $\frac{N_x}{N^*}$ both at the center of the plate and the middle of the support. The results for the center of the plate are presented in curves and tables; the results for the supports appear only in tabular form. Thus knowing ρ,η and N^*, fixed physical parameters, α,β and γ can be found from the tables or curves hence w, M_{x_o}, and M_{y_o} and finally the stresses.

PROCEDURE

In order to conduct an experiment to check Mansour's linearized solution of the orthotropic plate problem in a feasible manner, it was decided to limit testing to a representative bottom structure with a single set of boundary conditions and vary both lateral and in plane loads.

Design of the experimental test system was subdivided into four sub-systems:

(1) Test Specimen Subsystem

(2) Load Application Subsystem

(3) Support and Boundary Condition Subsystem

(4) Strain and Deflection Measurement Subsystem.

No involved attempt was made to optimize the test system other than trying to obtain the simplest solution at the least cost, since both time and money were somewhat limited.

The testing system chosen and implemented consists of a model of a bottom structure constructed from Plexiglas G which is loosely scaled from the double bottom of a Mariner class ship. Case III boundary conditions were used with the in plane loads applied by hydraulic jacks and normal loads applied by a pressurized rubber bag. The model was instrumented with fail strain gages to measure strain, and dial indicators were used in several locations to measure the deflection of the model and the boundary condition supports. Appendix A gives a detailed description of the entire test system.

The A.S.T.M. standard Young's modulus for Plexiglas G as given in Reference 15 is 450,000 psi for tension, compression and flexure. A preliminary experiment was conducted to determine the apparent modulus for Plexiglas G due to creep, and a five minute creep value of 410,000 psi was determined. The value of Poisson's ratio for Plexiglas G could not be found in manufacturer's literature or from other local references. Reference 7 lists a Poisson ratio for Perspex, also a polymethyl methacrylate plastic, of 0.35 and Braithwaite and Williams state in Reference 9 that if ν lies between 0.25 and 0.38, the maximum possible error in estimating stresses is 9 per cent. Therefore, a value of 0.35 was chosen as the Poisson ratio of Plexiglas G.

Testing was divided into two parts. The first set of tests was conducted with the boundary conditions shown in Figure 6 and 7 and with the following loadings:

$\frac{N_x}{N^*}$	0	0	0	0.055	0.055	0.055	0.055
q(mm)	30	60	90	52	64	104	147

The second set of tests was conducted with the modified boundary condition shown in Figure 9 and with the following loadings:

$\frac{N_x}{N^*}$	0	0	0	0	0	0	0	0.11	0.11	0.11
q(mm)	10	30	m 40	60	70	90	100	0	40	70

$\frac{N_x}{N^*}$	0.055	0.055	0.055	0.055	0.055	0.055	0.055	0.055
q(mm)	0	10	30	40	60	70	90	100

Each test consisted of loading the model, waiting for five minutes, and then recording strains and deflections.

RESULTS

Results of Group I and Group II tests are shown graphically in the following pages. Group I tests were conducted over a seven day period with various minor adjustments made to the boundary conditions. Initially Group I tests were performed as a trial-run, and there was no intention of having the results recorded in this thesis. However, the Group II tests, which were conducted after the final system modification, still indicated system problems so Group I tests are recorded for comparison.

The following results are recorded in addition to the graphical presentation:

(1) The model developed two cracks in vertical members during a set of Group I tests. The loading on the model when it cracked was q = 147mm and $\frac{N_x}{N^*} = 0.055$. The cracks started at the top of the centerline and starboard longitudinal stiffeners where the stiffeners join the top plate, and continued downward almost to the bottom of the stiffeners. The coordinates of the points where the cracks start are (6.1, 17.0) and (6.1, 23.5). Before Group II tests were conducted an attempt to repair the model was made by drilling small holes through the top plate and injecting CADCO #94 glue into the cracks with a hypodermic needle. This repair was partially successful--about 85% of the starboard crack and 20% of the centerline crack were reglued.

(2) Boundary condition members in Group I tests defected upward when a lateral load was applied to the model.

q (mm)	Deflection of center of transverse B.C.	Deflection of center of longitudinal B.C.
25	0.031"	0.030"
47	0.062"	0.063"
68	0.099"	0.096"

(3) Deflection of model center in Group II tests with transverse boundary conditions shown in Figure 9 and longitudinal boundary condition members removed (= free B.C.) were:

q (mm)	Wc
32	0.065"
64	0.125"

(4) Deflection of model longitudinal supports in Group II tests:

q (mm)	10	30	40	60	70	90	100
W (inches)	0	0.003	0.004	0.006	0.007	0.010	0.012

Deflections in (2), (3) and (4) were measured relative to the floor.

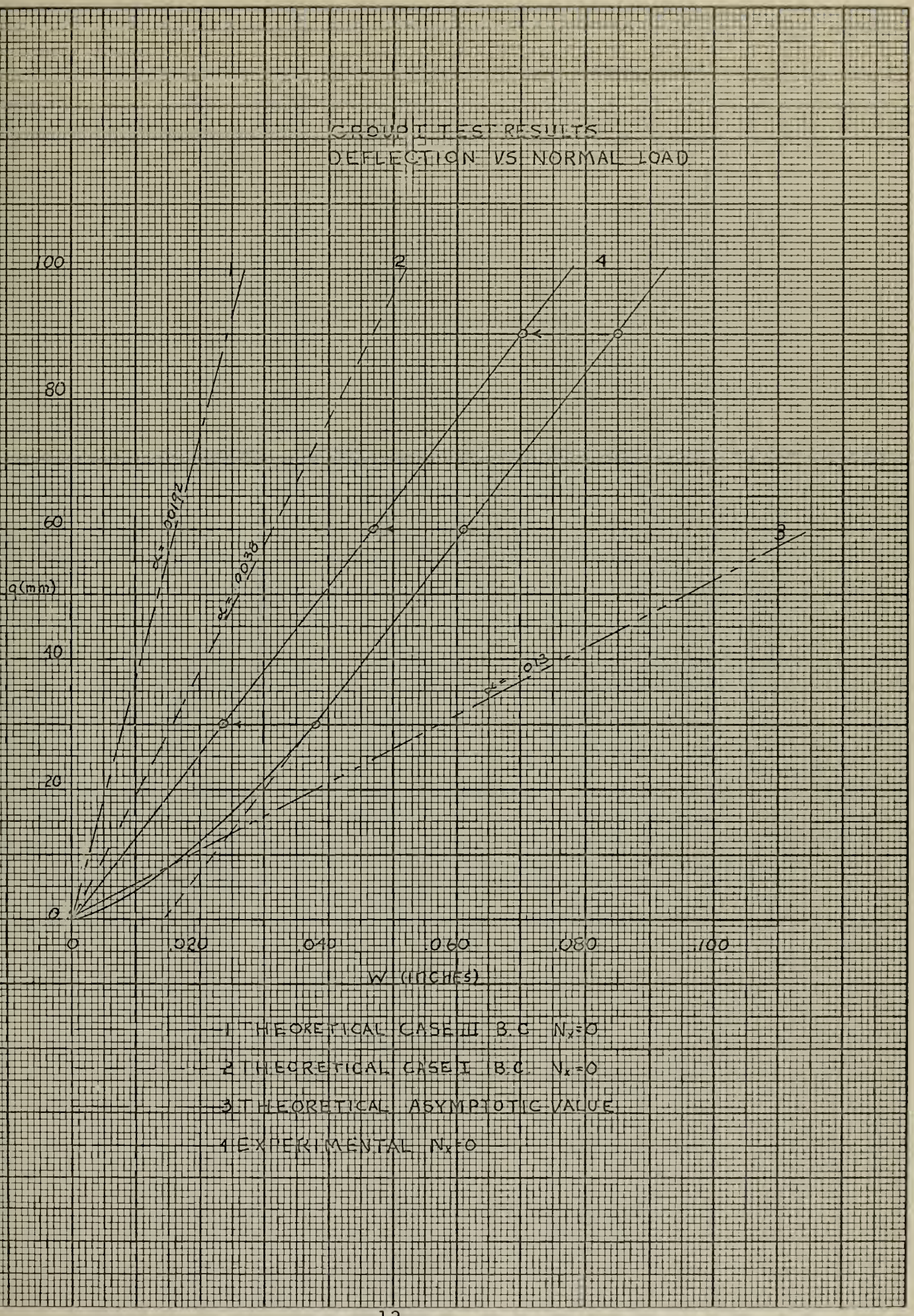
CROUT TEST RESULTS
DEFLECTION VS NORMAL LOAD
100
80
60
40
20
0
q(mm)
0
.020
.040
.060
.080
.100
W (INCHES)
1
2
3
4
a=.0112
a=.0136
a=.012
1 THEORETICAL CASE III B.C $N_x=0$
2 THEORETICAL CASE I B.C $N_x=0$
3 THEORETICAL ASYMPTOTIC VALUE
4 EXPERIMENTAL $N_x=0$

GROUP I RESULTS

X BENDING STRESS VS. NORMAL LOAD

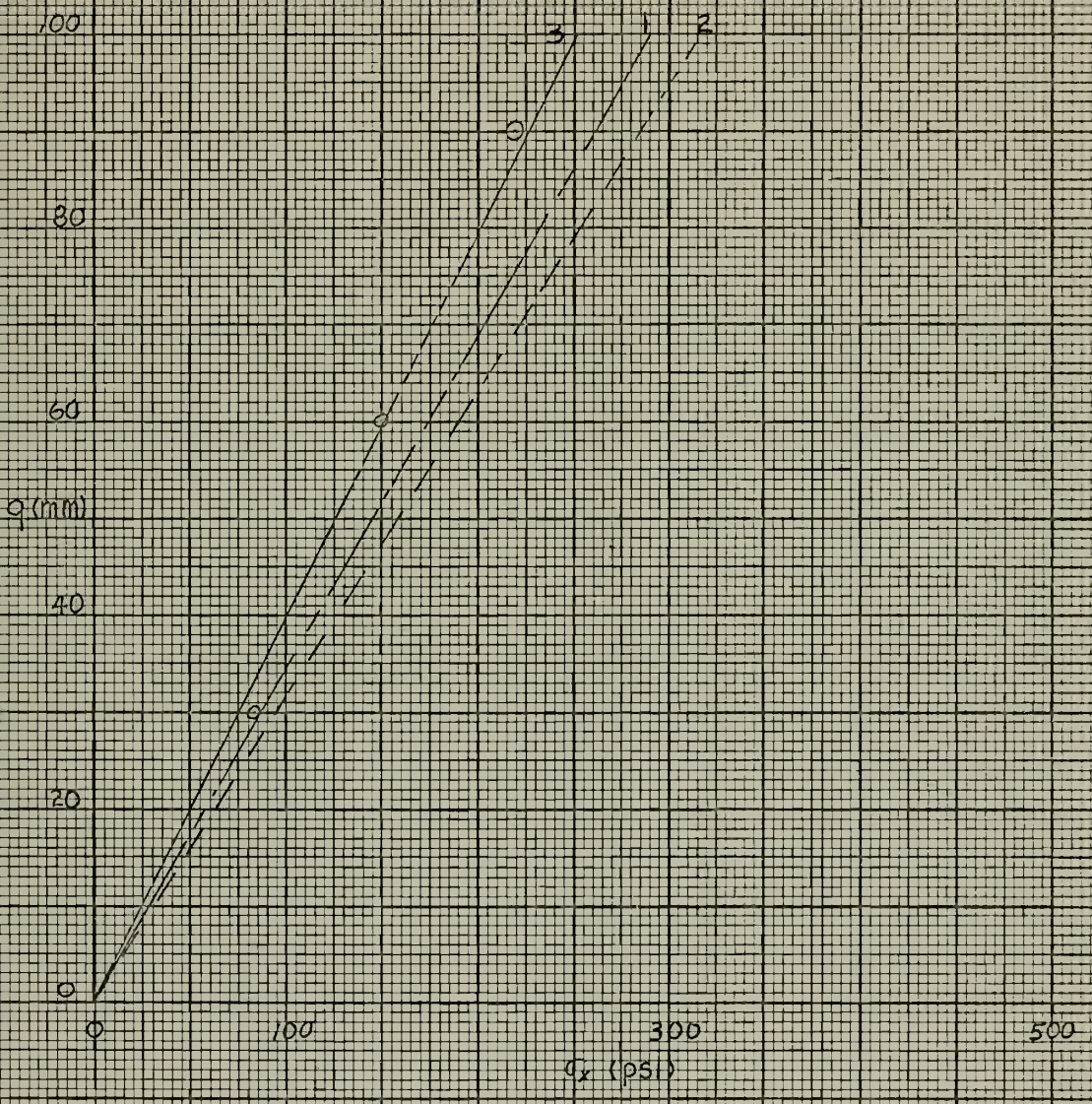

1 THEORETICAL CASE III B.C. $N_x = 0$

2 THEORETICAL ASYMPTOTIC VALUE

3 EXPERIMENTAL

GROUP I RESULTS

Y BENDING STRESS VS NORMAL LOAD

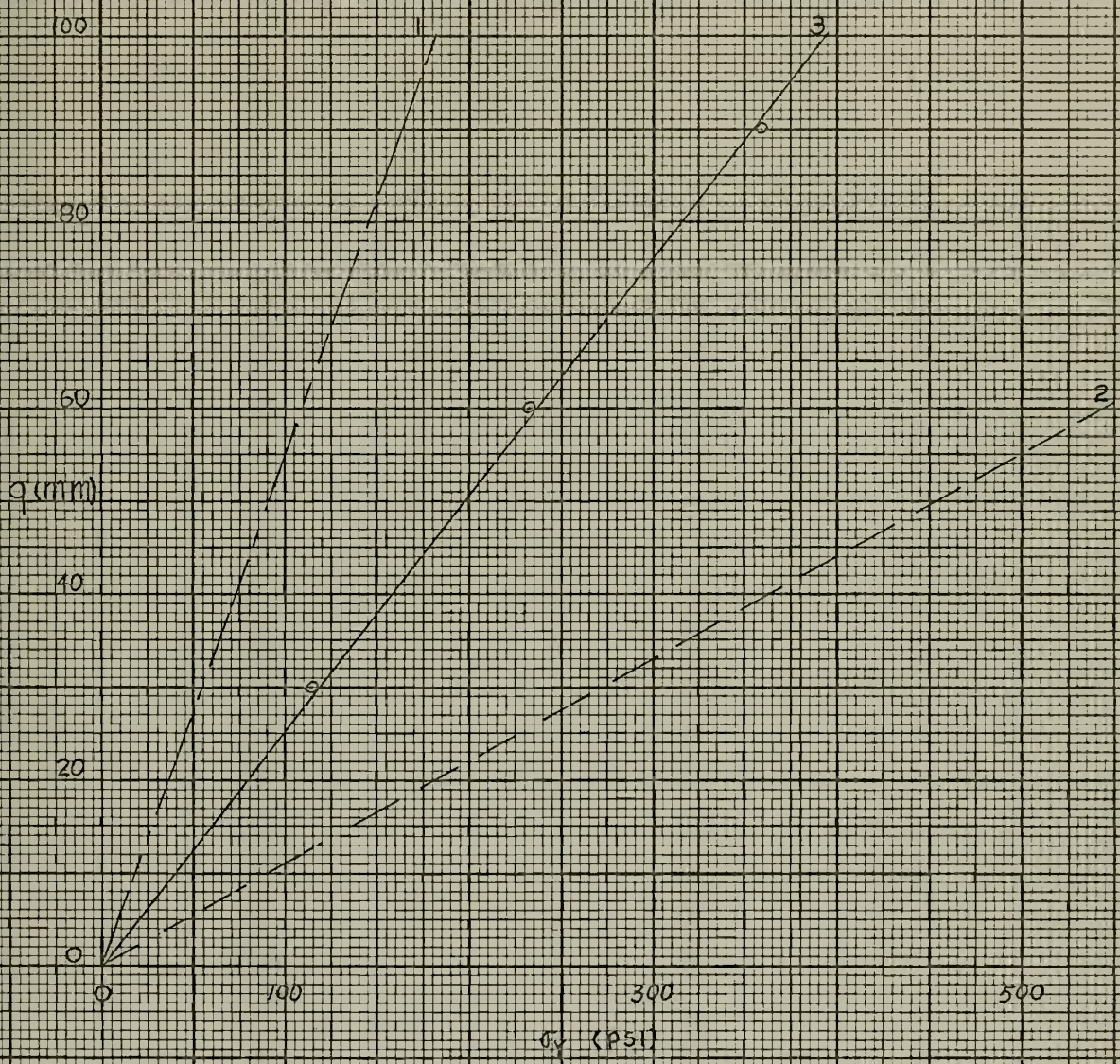

1 THEORETICAL CASE III B.C. $N_y = 0$

2 THEORETICAL ASYMPTOTIC VALUE

3 EXPERIMENTAL

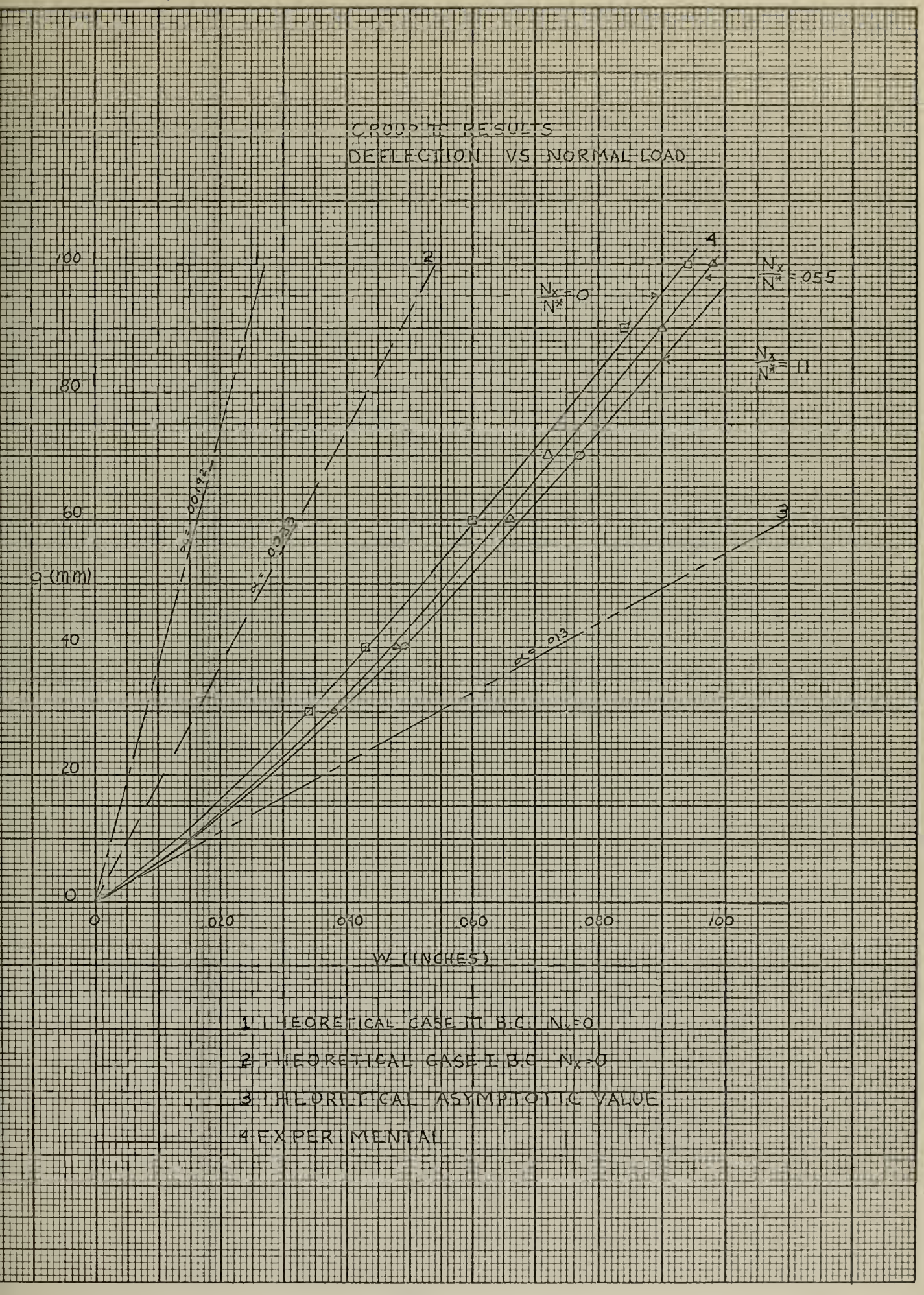
GROUP IC RESULTS
DEFLECTION VS NORMAL LOAD
100
80
60
40
20
0
q (mm)
0
020
040
060
080
100
W (INCHES)
1
2
3
4
$\frac{N_x}{N^*}=0$
$\frac{N_x}{N^*}=.055$
$\frac{N_x}{N^*}=.11$
$\alpha=.013$
1 THEORETICAL CASE III B.C. $N_x=0$
2 THEORETICAL CASE I B.C. $N_x=0$
3 THEORETICAL ASYMPTOTIC VALUE
4 EXPERIMENTAL

GROUP II RESULTS

X-BENDING STRESS VS NORMAL LOAD

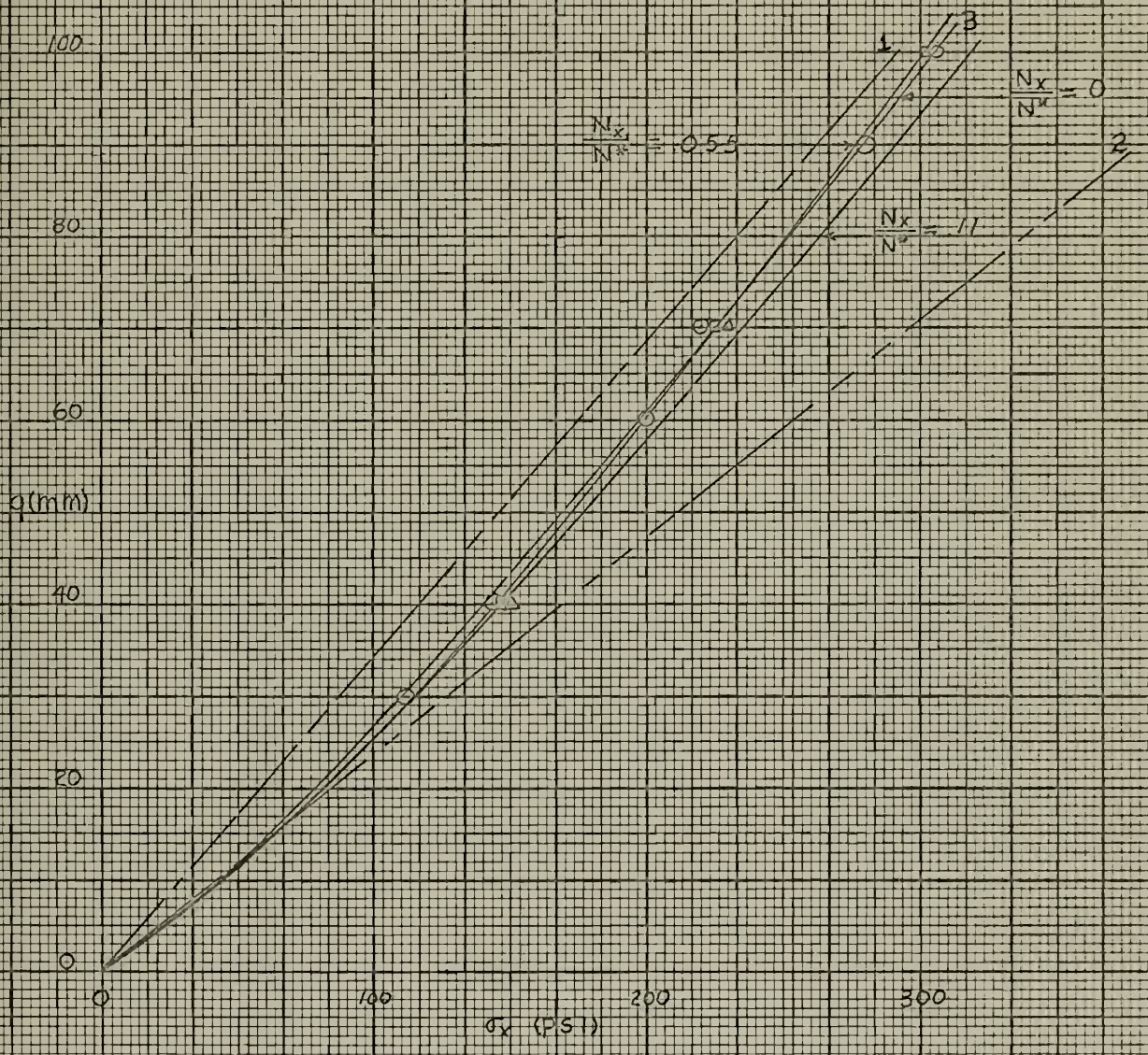

1 THEORETICAL CASE III BOUDARY CONDITIONS $N_y = 0$

2 THEORETICAL CASE I BOUNDARY CONDITIONS $N_x = 0$

3 EXPERIMENTAL

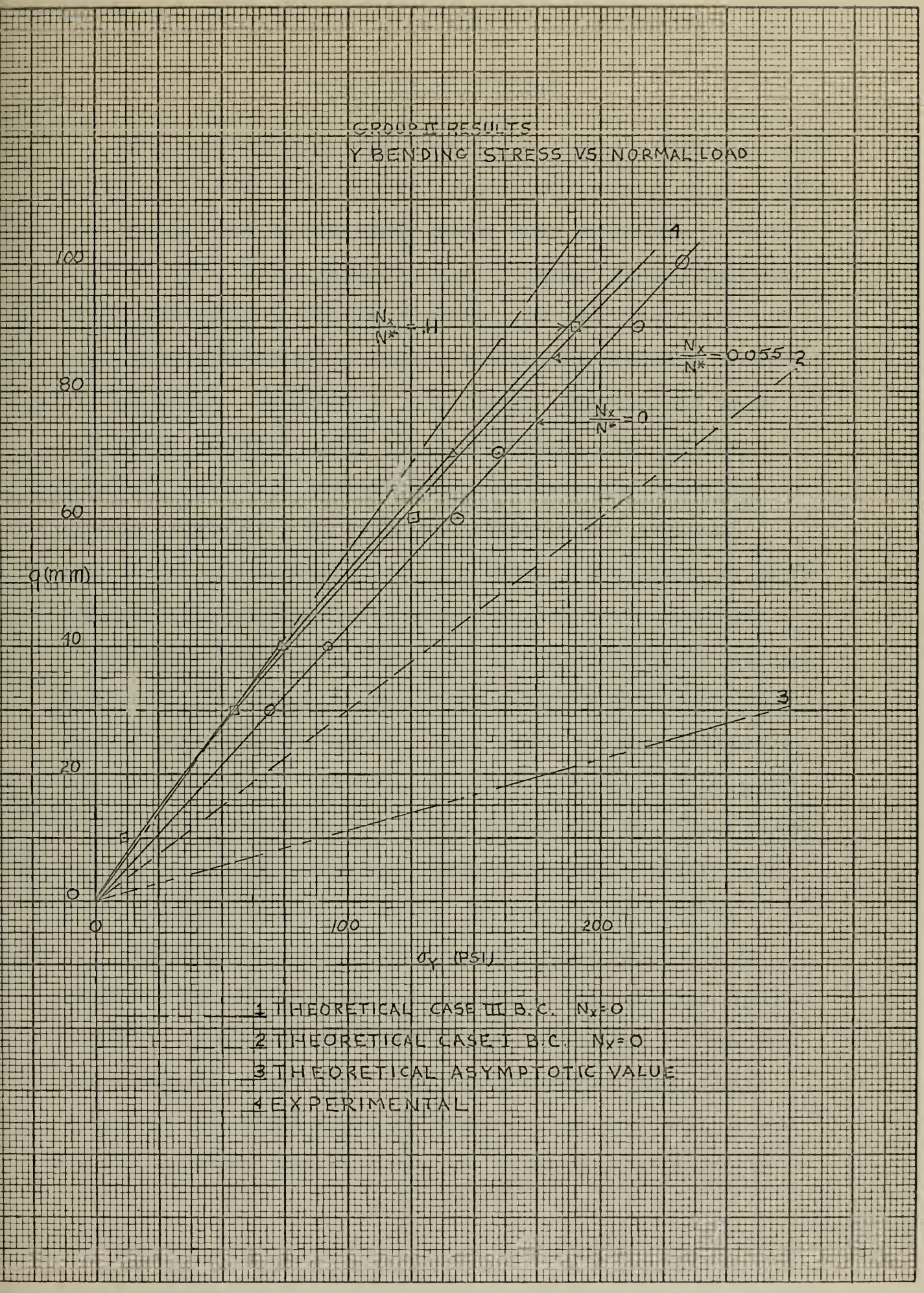
GROOP II RESULTS
Y BENDING STRESS VS NORMAL LOAD
100
80
60
40
20
0
q (mm)
0
100
200
σ_y (PSI)
$\frac{N_x}{N^*} = .11$
$\frac{N_x}{N^*} = 0.055$
$\frac{N_x}{N^*} = 0$
1
2
3
4
1 THEORETICAL CASE III B.C. $N_x = 0$
2 THEORETICAL CASE I B.C. $N_x = 0$
3 THEORETICAL ASYMPTOTIC VALUE
4 EXPERIMENTAL

DISCUSSION OF RESULTS

The experimental results did not compare favorably with those predicted from theory. Center deflection of the model was linear, but it was much larger than expected. I feel that a major factor contributing to larger than predicted model deflections was the inability of the transverse and longitudinal members to apply the desired boundary conditions to the model. As shown in the results section for Group I and Group II tests, both the longitudinal and transverse boundary condition members deflected when the model was loaded laterally. In addition, although not recorded, laboratory measurements for both Group I and Group II tests showed that the transverse boundary conditions rotated about their transverse axis. Thus, complete fixity was not achieved. For Group I tests, the supports deflected relatively more than the model. This large support deflection was the reason for shifting to the modified boundary conditions shown in Figure 9. It was hoped that by adding stiffeners, more rigid boundary conditions would result, and thus a closer approximation to the desired situation.

Accurate boundary conditions are very important in experimental analysis of structures because changes in the boundary conditions will affect the deflection surface and the stresses. Since the first condition for both simply supported and fixed boundary conditons is zero deflection at the boundary, the experimental conditions were not as

planned. The effect of boundary condition change can be seen both theoretically and experimentally. In theory, a change from Case III to Case I boundary conditions will approximately double the center deflection of the model. Experimentally, as shown in the results, the center deflection almost doubled when the longitudinal supports were removed, allowing a free end boundary condition along these sides. There is no way to tell what type of boundary conditions existed during the experiments. Even if there were, no theoretical solution exists, so no comparison could be made. However, it is possible to put theoretical bounds on the results expected. The lower bound is the theoretical solution for the planned Case III boundary condition, and the asymptotic solution for a cylindrical surface resulting from simply supported or fixed transverse ends and free longitudinal ends is the upper bound. Theoretical solutions for Case III, Case I and cylindrical surface boundary conditions are plotted on the deflection curves presented in the Results. The deflection curves obtained experimentally lie within the bounding conditions.

In the 0 - 25 mm range, the deflection curves are non-linear. This may be explained partially by the slack in the system. The clearance between the model and the boundary condition supports was kept to less than 0.010"; however, this clearance did vary and certainly some upward model movement occurred before there was an actual load on the model. If the linear portion of the deflection curve is

extended to the abscissa, an initial deflection of 0.012 - 0.016 inches results for all curves. The actual deflection curve could be redrawn, subtracting this initial amount and translating the curve to the left, so it starts from the origin. This would bring the results closer to those for the Case III boundary condition.

From the Results, center x and y bending stresses appear to be closer to the expected values than were the deflections. One would think that if the deflection is three times as large as predicted, perhaps the stresses should be, too. The apparent contradiction can be explained somewhat by the shapes of the α, β and γ curves. Both the α and γ curves (Figures 14 and 18 of Reference 5) for Case III boundary conditions, $\eta = 0.94$ and $\frac{N_x}{N^*}$ in the 0 - 0.1 range, start at a zero for $\rho = 0$ and increase constantly to asymptotic values at $\rho = 3.5$. The β curve starts at zero (Figure 16 of Reference 5) and increases to a maximum value at $\rho = 4.0$. Because of the shapes of the α and γ curves, it is possible to get upper and lower bounds for w and σ_{y_b}, but this is not possible for σ_{x_b}.

For Group I tests the transverse boundary conditions deflected a great deal, and the model needed to conform to the shape of the boundary conditions. The longitudinal boundary conditions did not deflect as much as the transverse conditions. The deflection values shown in the results section for Group I tests indicates the same deflection for transverse and longitudinal members; however, the longitu-

dinal members were attached to the transverse members so that relative to the model, the longitudinal members had a smaller deflection. With these deflected boundary conditions, I feel the model tended toward a cylindrical surface, the axis of the cylinder being in the longitudinal direction. This would help to explain the larger deflection, larger y bending stress and smaller x bending stress shown in the Group I test results.

For Group II tests the deflection of the boundary condition members was reduced significantly, but they still had a sizable deflection. σ_x and σ_y bending stresses more closely approximated the theoretical results than in Group I tests; however, the center deflection was about the same. It is not apparent to me why the change in boundary conditions improved the stresses but not the deflection. I do feel that Group II tests progressed toward the desired test conditions; however, the boundary conditions were still far from those planned. Because of the rotation, the transverse boundary conditions approached simple supports, and I think that possibly the effective length of the orthotropic plate was increased due to the rotation of these supports. If the effective length were increased from 30" to 36" and all the boundary conditions were simply supported, ρ would increase from 0.952 to 1.15, α from 0.00192 to about 0.0053, β from 0.029 to about 0.034 and γ from 0.016 to about 0.05. The expected results would be a much larger deflection, a slightly larger x direction bending stress and a much larger

y direction bending stress. For Group II tests, the deflection was much larger than theory and the x bending stress slightly larger, but the y direction bending stress was also only slightly higher.

The above attempts to explain the experimental results with orthotropic plate theory only point in a general direction of explanation. It can be concluded that: (1) exact boundary conditons are very important in experimentally determining stresses and deflections in an orthotropic plate, (2) that the desired fixed boundary conditions and simply supported boundary conditions were not achieved with the system design, and (3) that no verification of Mansour's orthotropic plate theory was possible from these experiments.

The model is outfitted with 25 strain gages and originally the plan was to plot stress distribution along the centerline of the model in the x and y directions along with comparing the center and support stresses with theory. The data in Appendix B shows that the strains were not symmetrical and followed no predictable pattern. Inplane loads did not distribute the stress completely throughout the model and only the top and bottom stresses at the transverse centerline were representative of the load applied. The inplane loading system was modified from two jacks in Group I tests to three jacks in Group II tests in order to get better load distribution. The distribution of inplane loads in Group II tests was better, but still not evenly distri-

buted. Another problem with the inplane load was the inability to accurately repeat the same load. This was caused by the insensitivity of the hydraulic pressure gage. The gage was calibrated in 20 pound increments and a 10 psi change in hydraulic pressure caused a variation in N_x of 4.5 lbs./in.

Lateral loads from the air bag distributed quite well; but, due to rotation of the transverse boundary conditions, the strains at the supports were lower than expected. Also the support strains are not symmetrical, indicating different amounts of rotation in each support. Since the support strains were not symmetrical or close to predictable, the corresponding stresses were not recorded.

Originally it was planned to load the model up to 154mm normal load and an inplane load corresponding to $\frac{N_x}{N^*} = 0.5$. After the model cracked, the maximum loads applied were q = 100mm and $\frac{N_x}{N^*} = 0.11$. The model seemed to perform just as well after the cracks developed as before. Strains and deflections from the same loads and boundary conditions corresponded very well, and it was concluded that the model was still good for reduced loads. Tensile strength of plexiglas is 9,000 psi, compressive strength is 13,000 psi and flexure strength is 17,000 psi.[15] The loading which caused the model to crack should not have caused stresses anywhere close to the magnitudes required for fracture. The cracks must have resulted from notches or defects in the vertical members.

The plexiglas model had many advantages and I feel that if it were not for the indeterminate nature of the boundary conditions, orthotropic plate theory could have been verified using this model. It was lightweight, easy to handle and transparent. Transparency was a great characteristic because it afforded inspection of the model structure, strain gages and the air bag before, during and after tests. Some creep was noticed as the model was loaded, especially after a long time loading, but the creep was never more than 8 - 10% and could be predicted.

CONCLUSIONS

(1) Plexiglas if a good material for models used in experimental stress analysis, provided results in the linear elastic range are desired.

(2) Applying correct boundary conditions is very important in experimental work with orthotropic plates.

(3) The desired fixed transverse and simply supported boundary conditions were not obtained.

(4) The inplane loading caused a non-uniform direct stress distribution in the plate, and only those direct stresses on the transverse centerline of the plate approximated theoretical stresses.

(5) No verification of Mansour's orthotropic plate theory can be made from this set of tests.

RECOMMENDATIONS

1. FAE-25-126SL strain gages are unidirectional and were difficult to align perpendicular to each other. When mutually perpendicular strains are desired, a type FAET-12A-12S9L strain gage or its equivalent should be used.
2. When ordering or constructing a plastic model for experimental stress analysis check the strength, Young's modulus and drying time of the adhesive to be used and insure it meets all system requirements.
3. The existing model of the ship's bottom structure is still good and it could be used in further attempts to verify Mansour's orthotropic plate theory.
4. The next set of tests to verify the orthotropic plate theory should start with simply supported boundary conditions. If these tests are satisfactory, then I suggest increasing the complexity of the boundary conditions to those attempted in this experiment.
5. The boundary conditions will need to be changed before further orthotropic plate tests are conducted with the existing supporting system. Although a more sophisticated attempt to stiffen the existing boundary conditions might work, I recommend a new approach to the boundary condition design. I feel a system that would allow the transverse and longitudinal supports to be one integral piece would remove the problem boundary condition align-

ment with the model. It would also alleviate rotation of the longitudinal boundary condition members. I also feel a loading arrangement that had the air bag above the model backed up by a suitably stiffened plate should be considered. This would allow the critical boundary condition members to be under the model with the possibility of using the floor for stiffening of these members. This recommendation should be coordinated with Recommendation #4.

6. To improve inplane load distribution in the model I recommend increasing the number of RC-121 jacks to five and changing the 0 - 2,000 psi gage to a 0 - 500 psi gage for greater pressure resolution. If this change doesn't work it may be necessary to use a greater number of smaller capacity hydraulic jacks.

7. Rigid polyvinyl chloride plastic is also an excellent material for structural models (Reference 7) and perhaps new models could be made from this material as well as Plexiglas.

REFERENCES

1. Schade, H.A., "Bending Theory of Ship Bottom Structure", Trans. S.N.A.M.E., Vol.46, pp. 176 - 190.

2. Schade, H.A., "Application of Orthotropic Plate Theory to Ship Bottom Structure", Proceedings of the Fifth International Congress for Applied Mechanics, 1938, pp. 140 - 144.

3. Schade, H.A., "The Orthogonally Stiffened Plate Under Uniform Lateral Load", Trans. A.S.M.E., Vol. 62, December 1940, pp.A143 - A146.

4. Schade, H.A., "Design Curves for Cross-Stiffened Plating Under Uniform Bending Load", Trans. S.N.A.M.E., Vol. 49, 1941, pp. 154 - 168.

5. Mansour, A., "Orthotropic Bending of Ship Hull Bottom Plating Under the Combined Action of Lateral and Inplane Loads", Report No. NA-66-2, Prepared for Maritime Administration under Contract MA-2620, University of California, January, 1966.

6. Russo, V.L. and Sullivan, E.K., "Design of the Mariner-Type Ship", Trans. S.N.A.M.E., Vol. 61, 1953, pp. 94 - 218.

7. Wallace, G., "Structural Model Analysis with Thermoplastics" Strain, Vol. 3, Number 3, July 1967.

8. Clarkson, J., "Steel or Plastic? The Choice of a Material for Small Scale Models of Naval Structures", European Shipbuilding, 1962.

9. Braithwaite, J.C. and Williams, R., "The Use of Scale Models in Predicting the Behavior of Complex Structures", N.C.I.E.S. Trans. Vol. 79, 1963, pp. 149 - 164.

10. Moe, J. and Tonnessen, A., "Model Experiments and Finite Element Analysis of Stress in an Open Ship", European Ship Building, No. 5, 1966, pp. 76 - 81.

11. Clarkson, J., "Small Scale Grillage Tests", Royal Institution of Naval Arch., Vol. 109, Number 2, April, 1967, pp. 197 - 205.

12. Young, A.G., "Ship-Plating Subjected to Loads Both Normal to and in the Plane of the Plate", Trans. of the Institution of Naval Architects, Vol. 99 (1957), pp. 578 - 597.

13. Schade, H.A., "The Effective Breadth of Stiffened Plating Under Bending Loads",Trans. S.N.A.M.E. Vol.59(1951)pp.403-420.

14. Glasfeld, R., "Design and Construction of a 42 Foot Ship Structural Model Testing Facility", Series 184, Issue 1, Institute of Engineering Research, University of California, Berkeley, February, 1962.

15. Technical Bulletin PL - 229i, Plastics Department of the Rohm and Haas Company.

16. Murray, W.M., "Basic Electric Circuits for Strain Gages", Notes from lecture series presented at M.I.T., July, 1969.

APPENDIX A

DESCRIPTION OF APPARATUS

A preliminary investigation of the test system revealed that the test specimen had interfaces with all the remaining sub-systems so it was developed first.

Test Specimen

In order to make the experiment as realistic as possible, an existing ship with double bottom construction, the Mariner, was chosen as a prototype. Since the maximum bending moment usually occurs amidships, a hold just forward of amidships and its bottom structure were chosen as the test area.[6] The dimensions and plating thickness of the hold shown in Figure 2 were modified to those in Figure 3 in order to have a symmetrical and orthogonal specimen. The non-dimensionalized design parameters ρ, η and $\frac{N_x}{N^*}$ were computed for the modified Mariner--see Appendix C. Since ρ, η and $\frac{N_x}{N^*}$ are non-dimensional the assumption was made that the model could be considered representative if these parameters were kept constant. To do this the outside dimensions of the model were scaled in the same proportion as the prototype. The plating thickness could not be scaled because it would become too thin, so 1/8 inch plating was chosen as a first try and ρ, η and $\frac{N_x}{N^*}$ were calculated. With the dimensions shown in Figure 4 and a loading of $\frac{N_x}{N^*} = 0.055$, ρ, η and $\frac{N_x}{N^*}$ were the same for the model and the prototype, and thus the model size was determined.

The choice of material and method of fabrication of the

model initially presented a big problem because of the model size and closed nature. The first thought was to make a steel model using silver soldered joints, but excessive model weight, chance for initial deflection of the steel, the inability to put the top on the model, and the size of the support system required for loading, caused the rejection of this idea. Plastic as a model material was considered next.

There are practical advantages in constructing a model with plastic. Plastic models can undergo wider ranges of deformation, and their lower elastic stiffnesses simplify the problems of providing a large support system and also reduce the size of the loads required. Plastics are easy to cut, shape and bond, so fabrication is much easier than with steel. References 7,8,9 and 10 discuss other experimenter's success, or lack of it, with such materials. The problems associated with plastic as a model material are: (1) creep is always present and its effect must be known for accurate results, (2) the modulus of elasticity of plastics changes with temperature and humidity, and (3) some plastics are not dimensionally stable (these should be avoided in structural models).

After further research and consultation with Professor McGarry of the Civil Engineering Department, the decision was made to use Plexiglas as a material for the model. Plexiglas was chosen because it has a relatively low creep rate, it is dimensionally stable, it is transparent, and it is readily available in the size required. Plexiglas is the

trade name of a polymethyl methacrylate plastic manufactured by the Rohm and Haas Company in Philadelphia, Pennsylvania, and is available locally at the Cadillac Plastic and Chemical Company in Somerville, Massachusetts. The model was constructed by the F.W. Dixon Company of Cambridge, Massachusetts.

The actual size of the model was larger than the size calculated to allow for the application of loads and boundary conditions. The model built was 44" long by 38" wide by 2 3/4" deep--all made from 1/8" thick material. The longitudinal members are continuous while the transverse members or floors are intermittent. Both the top and the bottom of the model are one continuous piece. Cadillac Plastic and Chemical Company Number 94 glue was used to join all the members except the top--the top was glued with acrylic adhesive P.S. 30, a supposedly slow-drying glue. However, as the glue was being applied to the longitudinal and transverse members in preparation for putting the top on the model, the model maker noticed that the glue was beginning to set and rushed to get the top on. Consequently, less than 100% contact was achieved in the bond between the stiffening members and the top. As a backup to the glued joints, small brass screws were attached through the top and bottom plates into the stiffening members.

Load Application

In plane load application was provided by hydraulic jacks pushing against a 4 x 4 WF I-Beam which butted against an edge

of the model and acted to distribute the load. The jacks were pressurized by a two-speed hydraulic hand pump with pressure being read from a 0 - 2,000 psi hydraulic pressure gage.

Jack Description

Manufacturer - Blackhawk Industrial Division

Model Number - RC-251

Capacity - 20 Tons

Effective Ram Diameter - 5.1572 Square Inches

Extended Height - 16 3/8 Inches

Collapsed Height - 11 5/6 Inches

Pump Description

Manufacturer - ENERPAC, Division of Power Industries, Inc.

Model Number - P-80

Reservoir Capacity - 140 Cubic Inches

The P-80 pump and assorted hydraulic fittings were purchased from R.H. Scales Company in Boston.

Lateral loading was provided by a rubber bag pressurized with compressed air. The dimensions of the bag are 30" x 34" x 4". The main concern in designing the bag was to insure full bag-model contact when the bag was fully inflated. The clearance between the model and the floor is 2 5/8", and based on experience at the University of California (see Reference 14) it was decided to make the air bag about one and one-half times as deep as the clearance for complete contact. The floor was used to reinforce the air bag because of its stiffness; also, this left the top of the model clear for deflection

indicators and observations. The bag was made by the Approved Rubber Corporation of Winthrop, Massachusetts, from a tough rubber and is fitted with a truck tire valve for pressurizing and deflating.

Air is supplied from a bottle of compressed air fitted with a double stage AIRCO oxygen pressure reducer. The AIRCO pressure reducer will reduce the pressure from 3,000 psi down to the 0 - 60 psi range; however, to more closely regulate the pressure, a needle valve was fitted into the outlet of the AIRCO reducer. Schematics of lateral and in plane loading systems are shown in Figure 5.

Supports and Boundary Condition Members

The support system shown in Figure 6 is the backbone of the testing system. The system consists of four 8 WF 31 I-Beams that are bolted together to make the enclosing test bed. Bolted onto the longitudinal supports are the brackets for the boundary condition members and the load distributor I-Beams. The support system is bolted, instead of welded, to enable it to be disassembled and stored when not in use. Because a total upward force of more than 3,000 pounds was anticipated from the air bag, the entire support system is bolted through brackets to the floor.

Four 5" x 1 3/4" channels 60" long with machined knife edges act as fixed transverse boundary conditions. Two 2 1/2" x 2 1/2" x 3/8" T's 30" long bolted onto the upper transverse channels act as simply supported longitudinal boundary conditions. Both the channels and the T's were shimmed to

align them with the model. See Figure 7.

Strain and Deflection Measurement

The model is instrumented with 25 strain gages positioned as shown in Figure 8. The strain gages used are produced by BLH Electronics, Inc. of Waltham, Massachusetts. The gage characteristics are:

Type - FAE-25-12S6L

Resistance - 120 Ohms

Gage Factor - 2.05

Gage Length - 0.250 Inches

The gages were cemented in place using Eastman 910 cement, generally considered excellent for room temperature applications.

To measure the strains, a Wheatstone Bridge strain gage circuit was used with an active gage in one arm of the bridge, a dummy gage in another arm of the bridge and the remaining arms being internal to the strain indicator. This active-dummy system allowed for temperature compensation which was necessary since the strain gages weren't temperature compensated for plastic.

The instruments used for strain measurement were the Model 206 B DIGITAL STRAIN INDICATOR and MODEL 306 B SWITCH AND BALANCE UNIT. Both instruments were manufactured by William T. Bean, Inc. of Detroit, Michigan.

During the first attempts to balance the gages, a continual drift on the strain indicator was noticed and the gages would not balance. The bridge supply voltage of the strain

indicator is 3.5 volts and, like most commercial instruments, cannot be varied. With the strain gage circuit indicated and a 3.5 volt bridge voltage, a 16 milliamps current was measured in the active arm. Plastics have a low thermal conductivity. The heat developed in the gages tends to accummulate in the region close to the gage causing local variations in modulus of elasticity, and hence the drift. To correct this problem, a 147 ohm, 1% tolerance, resistor was added in series with each gage. The resistor acted to cut the current more than half and thus the heat by a factor of four. With the resistors in the circuit, it was possible to balance the gages.

The addition of resistance in series with a strain gage acts to desensitize the gage. The strain indicated must then be multiplied by a factor to find the true strain.

True Strain = Factor x (indicated strain)[16]

$$\varepsilon = \frac{\frac{\Delta R}{R}}{\text{Gage Factor}} \qquad \left(\frac{\frac{\Delta R_T}{R_T}}{GF}\right) = Q_t\left(\frac{\frac{\Delta R_g}{R_g}}{GF}\right) \quad \text{where } Q_t = \frac{1}{1 + \frac{R_s}{R_g}}$$

$R_s = 147\Omega$

$R_g = 120\Omega$

$R_T = 267\Omega$

$G_F = 2.05$

$Q_t = 0.45$

Factor = 2.22

The sensitivity of the system could be regained if the gage

factor setting on the strain indicator were changed (lowered) to compensate for the added resistance. However, the required setting for this arrangement was a gage factor of 0.91 which was too low for the Model 206 B strain indicator, so the gage factor was set at 2.05 and the indicated strain corrected to true strain by multiplying by 2.22.

The modification of the boundary condition members shown in Figure 9 was made in an attempt to stiffen the members. The 8 WF 31 I-Beams used to stiffen the transverse members were bolted to existing brackets mounted on the support system. Metal spacers about 1" thick were fitted between these I-Beams and existing transverse members. 4 WF 13 I-Beams were tack welded onto the existing longitudinal T-bars and these bars were then bolted to the 8 WF 31 I-Beams.

APPENDIX B

The formulas shown below were used to calculate theoretical and experimental values of deflection and stress.

Theoretical (Reference 5)

$$w = \frac{\alpha q b^4}{D_y} \qquad w = 7.22\alpha q \text{ (inches)}$$

$$\sigma_{xb} = \frac{\beta'}{1-\nu^2} \frac{q b^2 r_a}{\sqrt{\frac{D_x}{E}\frac{D_y}{E}}} \qquad \sigma_{xb} = 4.6 \times 10^3 \beta' q \text{ (psi)}$$

$$\sigma_{yb} = \frac{\gamma'}{1-\nu^2} \frac{q b^2 r_b}{\frac{D_y}{E}} \qquad \sigma_{yb} = 3.9 \times 10^3 \gamma' q$$

	α	β	γ	β'	γ'
Case III B.C.	0.00192	0.0285	0.0158	0.033	0.024
Case I B.C.	0.0038	0.038	0.035	0.048	0.045
Asymptotic Case	0.013	0.0	0.12	0.036	0.12

Experimental

$$\sigma_x = \frac{E}{1-\nu^2}(\varepsilon_x + \nu\varepsilon_y) \qquad \sigma_y = \frac{E}{1-\nu^2}(\varepsilon_x + \nu\varepsilon_y)$$

SUMMARY OF DATA - GROUP I TESTS

$\frac{N_x}{N^*} = 0$	Strain in Microinches/in.			$\frac{N_x}{N^*} = 0.055$	Strain in Microinches/in.		
Gage	q=30	q=60	q=90	q=52	q=64	q=104	q=0
1	-11	-29	-29	-618	-535	-462	-641
4	+251	+515	+815	+682	+705	+1002	+285
5	+129	+206	+278	-422	-396	-143	-765
8	+22	+132	+244	-298	-170	-97	-382
11	-9	-21	-62	-	-840	-	-544
12	+362	+765	+1290	-	+1560	-	+179
14	-160	-373	-566	-	+37	-	+283
15	-133	-135	-224	-	-1250	-	-790
18	+62	+199	+362	-	-214	-	-222
25	-64	-112	-178	-810	-875	-	-651

$\frac{N_x}{N^*}$	0	0	0	0.055	0.055	0.055
q (mm)	30	60	90	52	64	104
w (inches)	0.038	0,061	0.085	-	0.064	0.048

CENTER STRESSES (PSI)

$\frac{N_x}{N^*}$	q(mm)	Top Stresses σ_x	Top Stresses σ_y	Bottom Stresses σ_x	Bottom Stresses σ_y	Ave. Bend. Stress σ_x	Ave. Bend. Stress σ_y
0	30	+90	+136	-78	-92	84	114
0	60	+177	+270	-122	-193	150	232
0	90	+254	+420	-194	-296	224	358
0.055	0	-303	+8	-318	0	310	4
0.055	52	-84	+247	-	-	-	-
0.055	64	-69	+261	+569	-188	219	221
0.055	104	+97	+438	-	-	-	-

SUMMARY OF DATA - GROUP II TESTS

$\frac{N_x}{N^*} = 0$ Strain in Microinches/Inch

Gage Number	q=10	q=30	q=40	q=60	q=70	q=90	q=100
1	-80	-175	-213	-338	-350	-448	-526
4	+7	+109	+164	+278	+316	+437	+490
5	+104	+217	+291	+338	+405	+465	+540
8	-16	+62	+118	+193	+147	+244	+178
11	+35	+98	+144	+200	+213	+286	+310
12	+151	+460	+675	+1000	+1195	+1575	+1865
14	+4	-22	-49	-91	-122	-142	-169
15	-98	-249	-304	-406	-436	-555	-630
18	0	+24	+166	+240	+355	+417	+178
25	+2	-111	-111	-224	-193	-333	-331

$\frac{N_x}{N^*} = 0.055$ Strain in Microinches/Inch

	q=0	q=30	q=40	q=60	q=70	q=90	q=100
1	-704	-731	-980	-888	-1100	-1070	-1271
4	+300	+328	+413	+496	+550	+635	+702
5	-918	-492	-585	-346	-450	-240	-300
8	-572	-521	-506	-406	-433	+393	-465
11	-526	-326	-278	-2]3	-150	-111	-7
12	+173	+736	+1017	+1448	+1680	+2143	+2315
14	+267	+235	+280	+202	+233	+169	+190
15	-745	-895	-1060	-1075	-1225	-1271	-1380
18	-342	-147	-78	+49	+111	+211	+295
25	-660	-635	-815	-718	-940	-925	-1078

SUMMARY OF DATA - GROUP II TESTS

$\frac{N_x}{N^*}$ = 0.11 Strain in Microinches/Inch

	q=10	q=40	q=70
1	-1150	-1340	-1518
4	+557	+635	+817
5	-1269	-1045	-990
8	-1465	-1430	-984
11	-900	-705	-677
12	-480	+1298	+2218
14	+547	+533	+512
15	-1408	-1660	-1880
18	-290	-506	-302
25	-1040	-1200	-1388

$\frac{N_x}{N^*}$ = 0

q	10	30	40	60	70	90	100
w	0.014	0.034	0.043	0.060	0.070	0.084	0.094

$\frac{N_x}{N^*}$ = 0.055

q	0	10	30	40	60	70	90	100
w	0	0.014	0.038	0.047	0.066	0.072	0.090	0.098

$\frac{N_x}{N^*}$ = 0.11

q	0	10	40	70
w	-0.099	0.006	0.040	0.077

SUMMARY OF DATA - GROUP II TESTS

CENTER STRESSES (PSI)

$\frac{N_x}{N^*}$	q (mm)	Top Stresses		Bottom Stresses		Ave. Bend. Stress	
		σ_x	σ_y	σ_x	σ_y	σ_x	σ_y
0	10	+47	+23	-41	-7	43	15
0	30	+117	+85	-118	-50	117	68
0	40	+147	+115	-139	-68	143	92
0	60	+200	+182	-201	-107	200	144
0	70	+220	+200	-220	-119	220	160
0	90	+283	+276	-278	-155	280	215
0	100	+305	+295	-307	-169	306	232
0.055	0	-353	-9	-287	0	0	5
0.055	10	-278	+8	-290	-14	9	11
0.055	30	-173	+72	-376	-36	100	54
0.055	40	-191	+93	-416	-39	145	61
0.055	60	-78	+172	-479	-80	199	126
0.055	70	-112	+171	-494	-85	244	128
0.055	90	-8	+253	-560	-127	277	190
0.055	100	-23	+258	-570	-127	304	193
0.11	10	-495	+51	-560	+25	33	38
0.11	40	-379	+127	-678	-21	129	74
0.11	70	-324	+217	-780	-67	228	142

APPENDIX C

Sample Calculation

The following calculations of ρ, η, $\frac{N_x}{N^*}$, w and σ_x for the modified Mariner bottom structure illustrate the use of Mansour's design curves.

From Figure 3. a = 60' and b = 68'

Section x-x

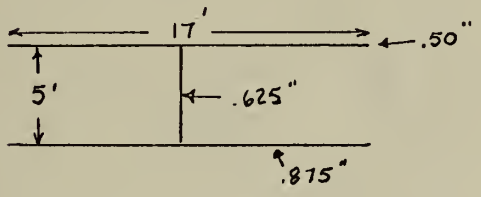

Section y-y

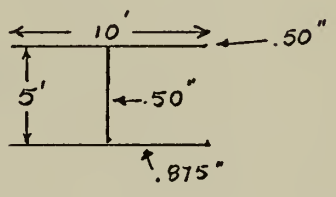

Neutral Axis for Section x-x is 23.5 inches from the bottom.
Neutral Axis for Section y-y is 23.8 inches from the bottom.

The effective breadth of section x-x is found from Schade's curve in Reference 13, for fixed end conditions, to be 74% of total width. For section y-y effective breadth is 105%.

New x-x Section

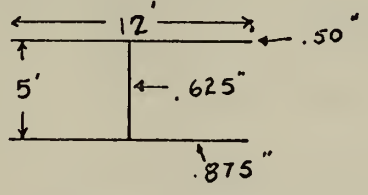

New y-y Section

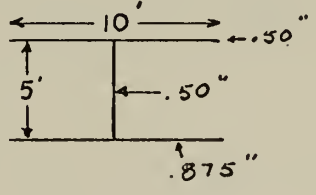

$I_x = 1327$ in.^{2} ft.^{2}

$I_{px} = 1249$ in.^{2} ft.^{2}

$I_y = 1088$ in.^{2} ft.^{2}

$I_{py} = 1025$ in.^{2} ft.^{2}

I_{px} and I_{py} are moments of inertia of top and bottom plating only.

$$D_x \approx \frac{EI_x}{S_a} \qquad S_a = 17' \text{ - spacing between longitudinals}$$

$$D_x = 2.81 \times 10^{10} \ \frac{\text{lb. in.}^2}{\text{in.}}$$

$$D_y \approx \frac{EI_y}{S_b} \qquad S_b = 10'$$

$$D_y = 3.91 \times 10^{10} \ \frac{\text{lb. in.}^2}{\text{in.}}$$

$$\rho = \frac{a}{b}\sqrt[4]{\frac{D_y}{D_x}} = \frac{60}{68}\sqrt[4]{\frac{3.91}{2.81}} = 0.962$$

$$\eta = \frac{H}{\sqrt{D_x D_y}} \approx \sqrt{\frac{I_{px} I_{py}}{I_x I_y}} = 0.935$$

$$N^* = \frac{\pi^2\sqrt{D_x D_y}}{b^2} = \frac{220 \text{ Tons}}{\text{In.}}$$

From Reference 6 Section Modulus, S, of the Mariner is 51,100 in.^{2}ft. Bending moment at a full load draft of 31.5' is 408,600 ft.-tons.

$$N_x = \frac{M}{S}\left(\frac{A}{b} + h\right) = \frac{408,600}{51,100}\left(\frac{5(37.5)}{68 \times 12} + 1.375\right) = 12.7 \text{ Tons}$$

$\left(\frac{A}{b} + h\right)$ is the equivalent plate thickness.

h is the combined thickness of the top and bottom plate.

A is the total area of the vertical plating.

$$\frac{N_x}{N^*} = \frac{12.7}{220} = 0.055$$

With $\rho = 0.962$, $\eta = 0.935$ and $\frac{N_x}{N^*} = 0.055$, the design curves

are entered for values of α, β and γ at the plate center.

$\alpha = 0.002$, $\beta = 0.029$ and $\gamma = 0.016$.

For a bending moment of 408,600 foot-tons and a uniform pressure load corresponding to a full load draft of 31.5', stresses and deflections are:

$$w = \frac{\alpha q b^4}{D_y}$$

$$w = \frac{(0.002)\left(\frac{31.5 \times 64}{144}\right)(68 \times 12)^4}{3.91 \times 10^{10}}$$

$$w = 0.316 \text{ Inches}$$

Stresses in Top Plating

$$\sigma_x \text{ bending} = \frac{\beta' q b^2 r_a}{1-\nu^2\sqrt{\left(\frac{D_x}{E}\right)\left(\frac{D_y}{E}\right)}} \qquad \beta' = \beta + \nu \frac{D_x}{D_y}\gamma$$

$$\beta' = 0.029 + 0.3 \frac{2.81}{3.91} (0.016)$$

$$\beta' = 0.0334$$

$$\sigma_x \text{ bending} = \frac{0.0334}{0.91} \frac{(14.0)(68 \times 12)^2 (37.38)}{\left[\frac{(2.81)(3.91) \times 10^{20}}{9 \times 10^{14}}\right]^{\frac{1}{2}} \times 2240}$$

$$\sigma_x \text{ bending} = +1.74 \frac{\text{tons}}{\text{in.}^2}$$

$$\sigma_t = \sigma_{xb} + \frac{N_x}{h \text{ equivalent}}$$

$\sigma_t = 1.74 + \frac{12.7}{1.6}$ For sagging condition

$\sigma_t = 9.69 \frac{\text{tons}}{\text{in.}^2}$ Top plating in sagging condition

FIGURE 1

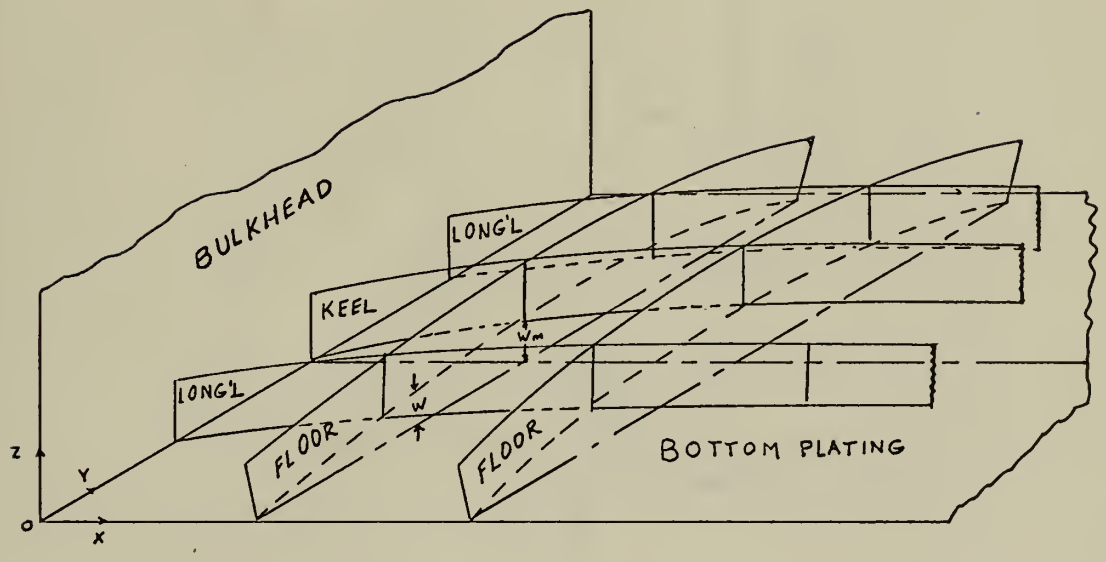

IDEALIZED SHIP BOTTOM DEFLECTED UNDER BENDING LOADS

FIGURE 2

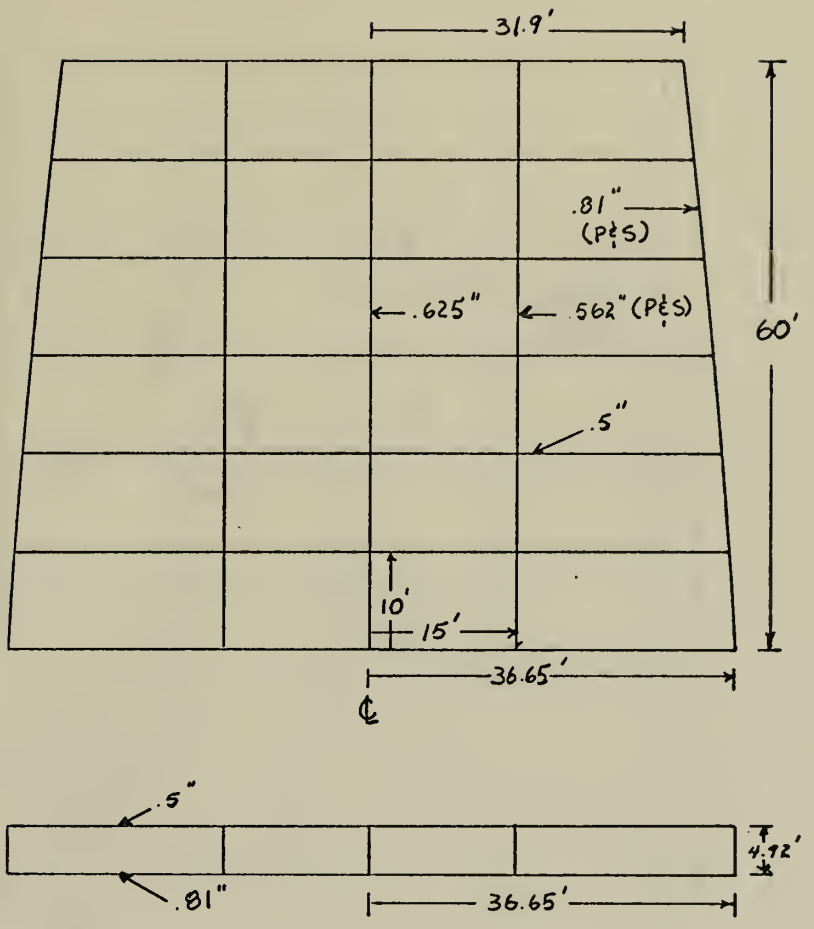

HOLD #4 MARINER CLASS CARGO SHIP

All dimensions and scantling locations taken from Ref. 6 with the exception of floor spacing, which was not indicated. Ten foot floor spacing was chosen because it seemed most reasonable and consistent with other ships.

FIGURE 3

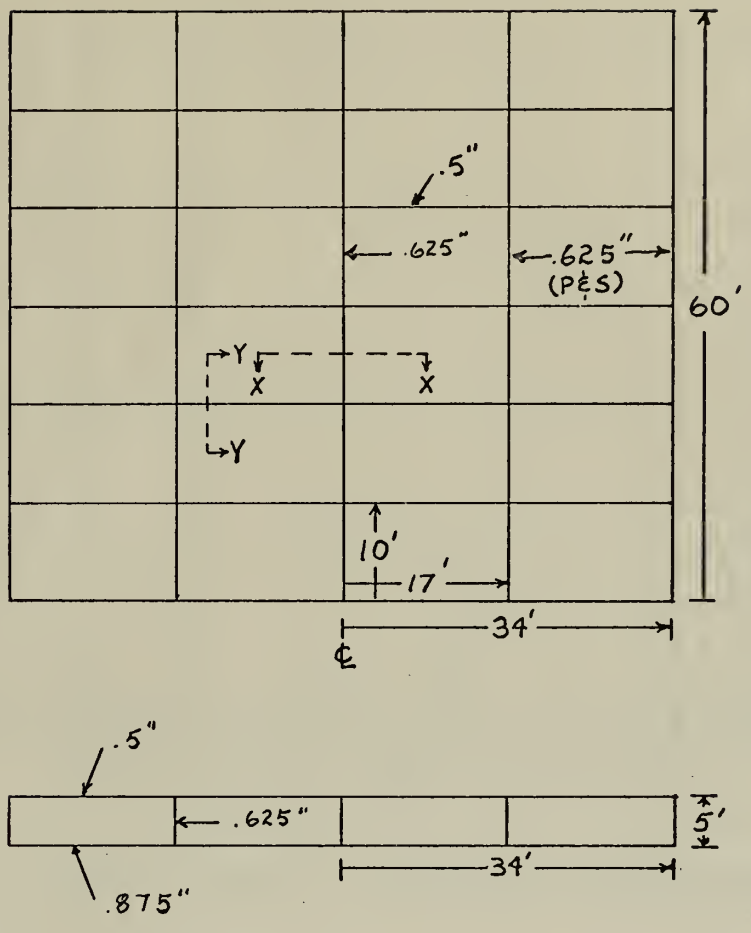

MODIFIED HOLD #4 MARINER CLASS

a = 60 feet

b = 68 feet

FIGURE 4 -

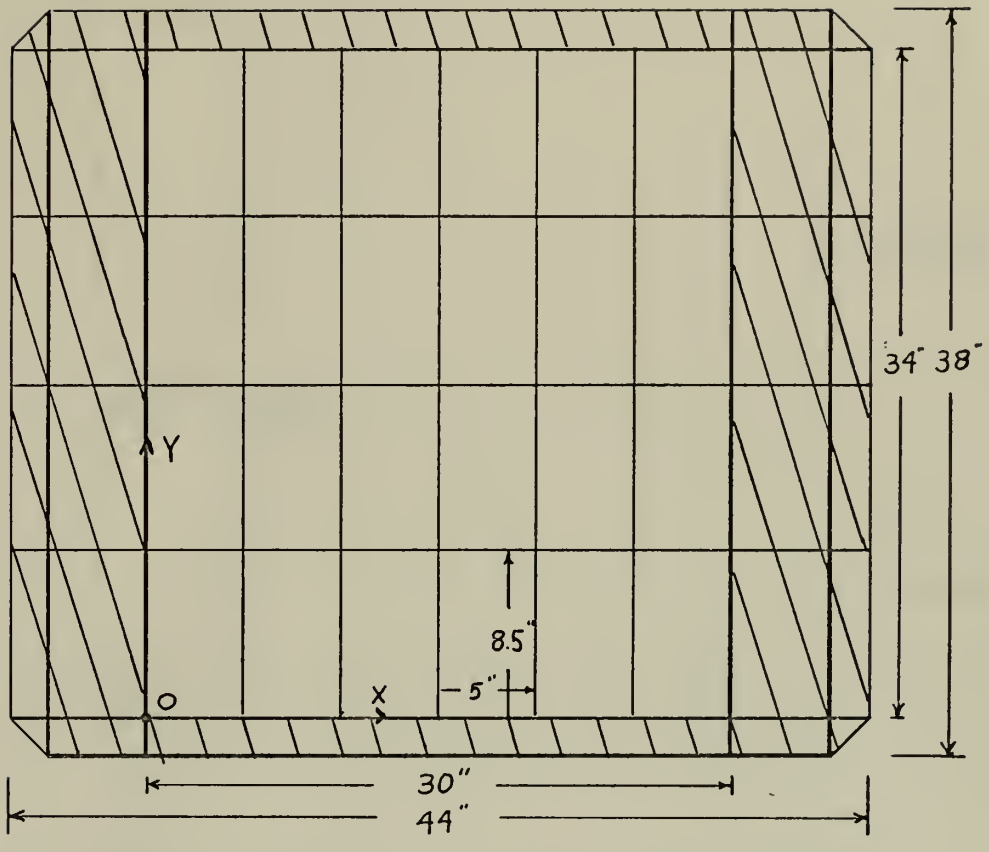

PLAN VIEW OF MODEL - DIAGONALS SHOW BOUNDARY CONDITION AREA

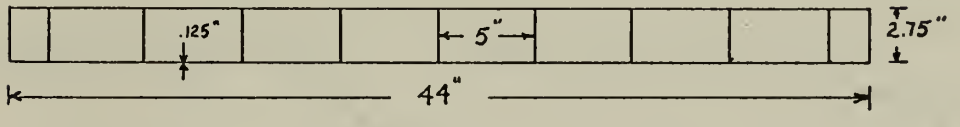

ELEVATION OF MODEL - ALL PLATE .125" THICK

FIGURE 5

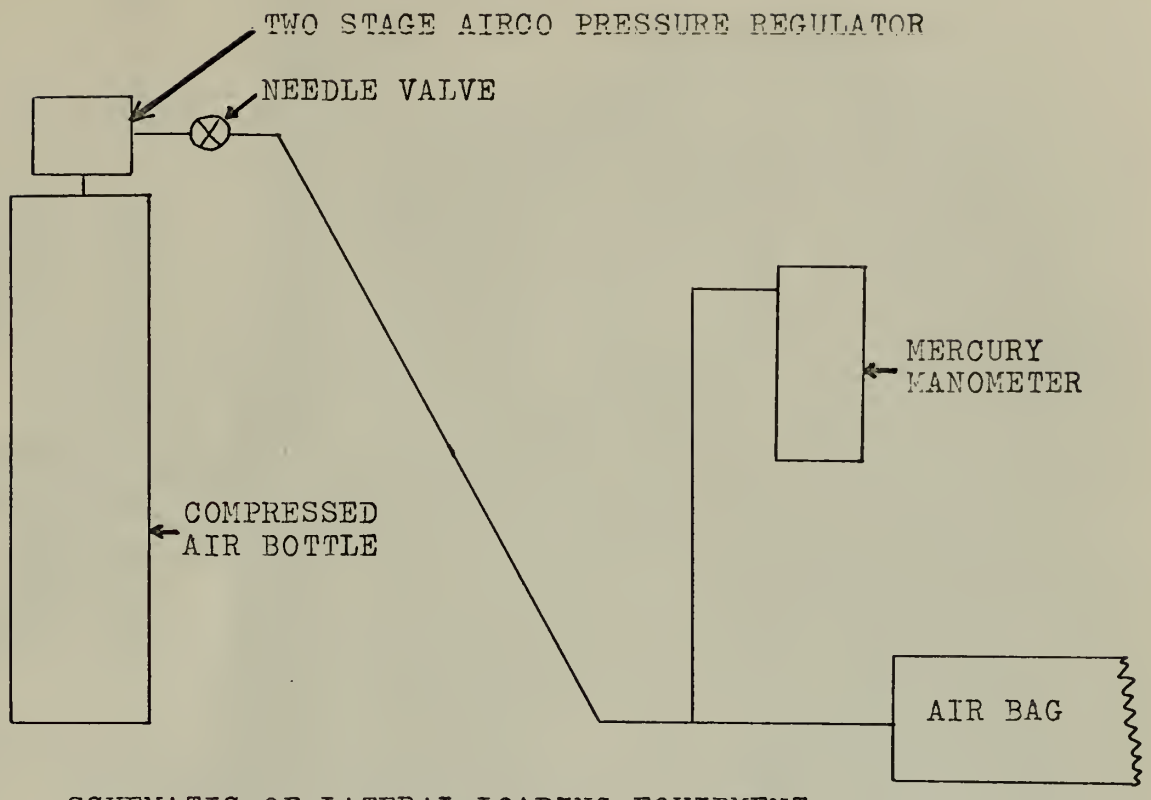

SCHEMATIC OF LATERAL LOADING EQUIPMENT

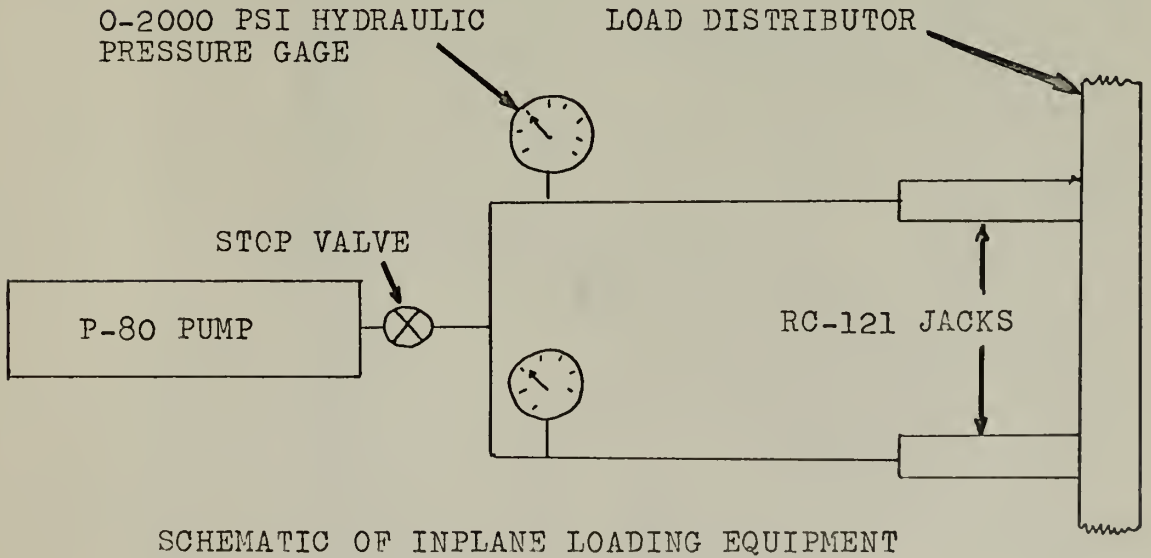

SCHEMATIC OF INPLANE LOADING EQUIPMENT

FIGURE 6

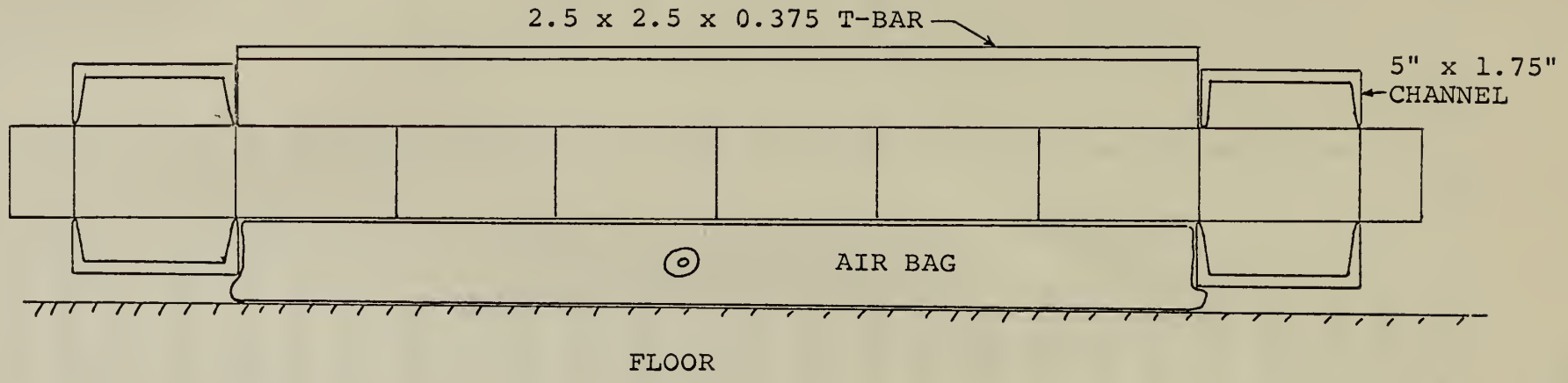

ELEVATION SHOWING BOUNDARY CONDITION APPLICATION AND AIR BAG--
CHANNELS AND T-BARS WERE MACHINED AND FILED TO PRESENT ROUNDED
KNIFE EDGES TO THE MODEL SURFACE

FIGURE 7

FIGURE 8

Gage #	Direction	Coordinates	Location
1	X	(29.5,17)	top, outside
2	Y	(22.5,17)	"
3	X	(22,17)	"
4	Y	(15.5,17)	"
5	X	(15,17)	"
6	X	(7.5,17)	"
7	Y	(7,17)	"
8	X	(.5,17)	"
9	Y	(20,25.5)	"
10	X	(20.5,25.5)	"
11	X	(29.5,17)	bottom, outside
12	Y	(22.5,17)	"
13	X	(22,17)	"
14	Y	(15.5,17)	"
15	X	(15,17)	"
16	X	(7.5,17)	"
17	Y	Broke after installation	
18	X	(.375,17)	bottom, outside
19	Y	(20.5,25.5)	"
20	X	(20,25.5)	"
21	Y	(23,18)	bottom, inside
22	X	(22.4,18)	"
23	Y	(22.5,18)	top, inside
24	X	(22,18)	"
25	X	(15,34)	side, outside on nuetral axis

FIGURE 9

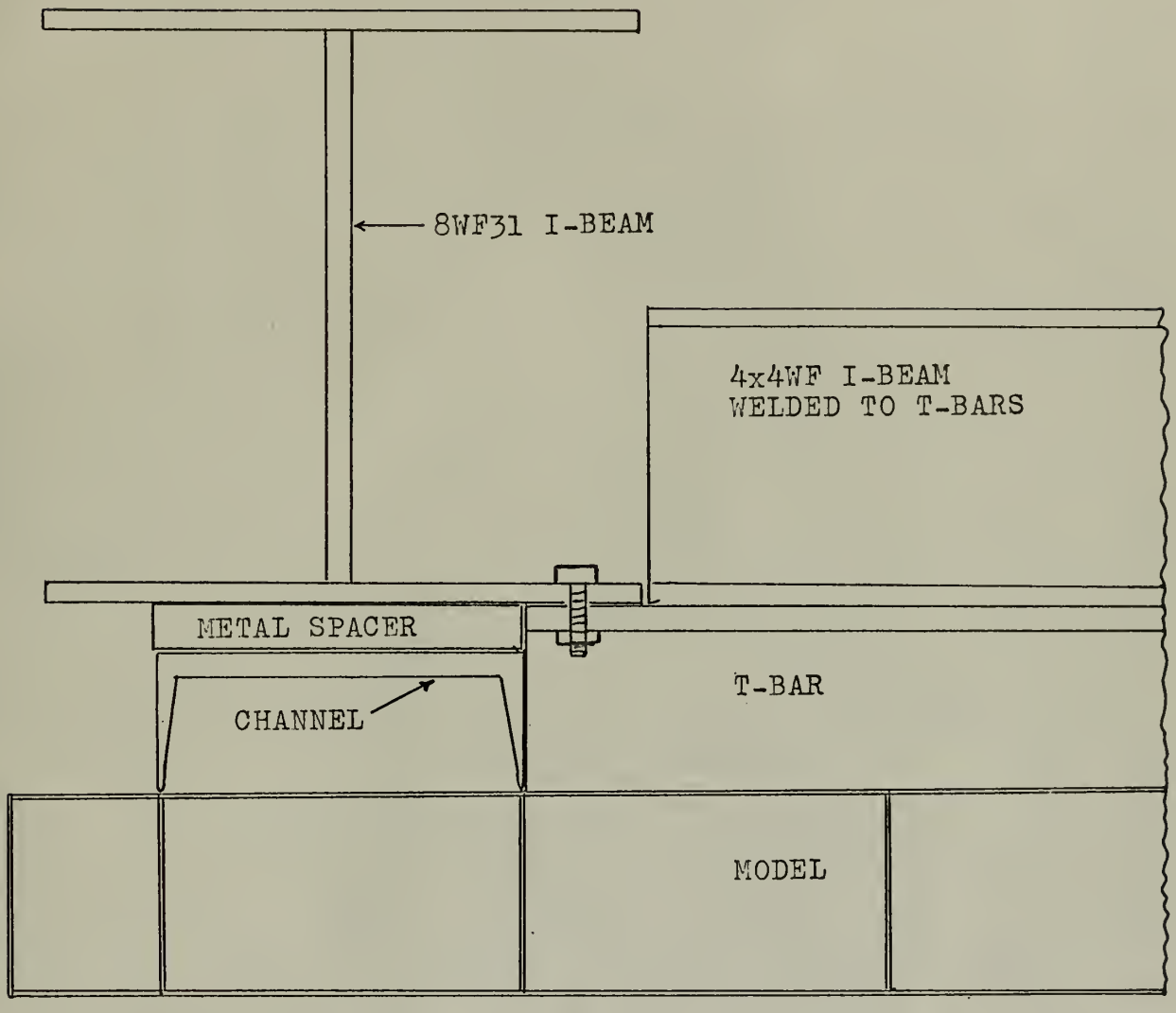

ELEVATION SHOWING TOP BOUNDARY CONDITION MEMBERS AFTER MODIFICATION

Thesis 118372
C197 Card
Experimental determination of stresses in a ship's bottom structure